The Impact of Clouds on the Shortwave Radiation Budget of the Surface–Atmosphere System: Interfacing Measurements and Models

ROBERT D. CESS AND SETH NEMESURE

Institute for Terrestrial and Planetary Atmospheres, State University of New York, Stony Brook, New York

ELLSWORTH G. DUTTON AND JOHN J. DELUISI

Climate Monitoring and Diagnostics Laboratory, Environmental Research Laboratories/NOAA, Boulder, Colorado

GERALD L. POTTER

Lawrence Livermore National Laboratory, Livermore, California

JEAN-JACQUES MORCRETTE

European Centre for Medium-Range Weather Forecasts, Reading, Berkshire, England

(Manuscript received 17 December 1991, in final form 1 May 1992)

ABSTRACT

Two datasets have been combined to demonstrate how the availability of more comprehensive datasets could serve to elucidate the shortwave radiative impact of clouds on both the atmospheric column and the surface. These datasets consist of two measurements of net downward shortwave radiation: one of near-surface measurements made at the Boulder Atmospheric Observatory tower, and the other of collocated top-of-the-atmosphere measurements from the Earth Radiation Budget Experiment. Output from the European Centre for Medium-Range Weather Forecasts General Circulation Model also has been used as an aid in interpreting the data, while the data have in turn been employed to validate the model's shortwave radiation code as it pertains to cloud radiation properties. Combined, the datasets and model demonstrate a strategy for determining under what conditions the shortwave radiative impact of clouds leads to a heating or cooling of the atmospheric column. The datasets also show, in terms of a linear slope-offset algorithm for retrieving the net downward shortwave radiation at the surface from satellite measurements, that the clouds present during this study produced a modest negative bias in the retrieved surface flux relative to that inferred from a clear-sky algorithm.

1. Introduction

There is a need to improve our knowledge of cloud–climate interactions, because cloud feedback is poorly depicted by current general circulation models. Although GCMs are the most comprehensive models for the purpose of projecting climatic change caused by increasing concentrations of greenhouse gases, cloud–climate interactions simulated by these models must be improved if they are ultimately to be used as reliable climate predictors (Cess et al. 1990).

The availability of data from the Earth Radiation Budget Experiment (ERBE) has provided unique insights into certain aspects of cloud–climate interactions (Ramanathan et al. 1989; Harrison et al. 1990). This was accomplished by separately averaging clear-sky, top-of-the-atmosphere (TOA) radiative flux measurements so that the TOA radiation budget with clouds present could be compared to that without clouds. The purpose of the present study is to demonstrate how such TOA measurements, when collocated with near-surface measurements, can enhance our understanding of how clouds impact the shortwave (SW) radiation budget of the surface–atmosphere system. For example, under what conditions do clouds either radiatively heat or cool the column? To demonstrate a procedure for addressing this issue, ERBE SW pixel measurements have been collocated with near-surface SW measurements made at the Boulder Atmospheric Observatory (BAO) tower. Output from the European Centre for Medium-Range Weather Forecasts (ECMWF) GCM was employed as an aid in interpreting the combined data, while the data were in turn used to validate one aspect of SW cloud parameterizations in the ECMWF GCM.

A related objective of this study was to employ the collocated tower/ERBE data to investigate the role of clouds on a retrieval algorithm for determining from

Corresponding author address: Dr. Robert D. Cess, Institute for Terrestrial and Planetary Atmospheres, State University of New York, Stony Brook, NY, 11794-2300.

SW TOA satellite measurements the net downward SW radiation at the surface.

2. Datasets

The collocation of ERBE SW satellite measurements with near-surface SW measurements made at the BAO tower is discussed in detail by Cess et al. (1991). The tower is located at 40.048°N, 105.008°W, about 25 km north of Denver. Net downward near-surface SW radiation was obtained by differencing measurements made from upward- and downward-facing pyranometers mounted on a 3-m boom extending from the tower's top level (300 m). Net downward SW radiation at the TOA is determined from measurements made by SW cross-track scanners on two satellites: the Earth Radiation Budget Satellite (ERBS), whose orbit has a 57° inclination angle relative to the equator, and *NOAA 9*, which is in a sun-synchronous polar orbit with an equator crossing time of about 1430 LT. ERBS data will mainly be used in this study because its inclined orbit provides sampling of each local hour every 36 days.

There are two sampling problems associated with the collocated ERBE and tower data. One is spatial sampling: the scanner pixels are roughly circular in shape with nadir diameters of about 35 km for ERBS and 50 km for *NOAA-9*, and these are considerably larger than the area viewed by the downward-facing tower pyranometer. As demonstrated by Cess et al. (1991) this poses no problem for clear conditions, because the terrain surrounding the tower is representative of that below the tower. Dutton (1990) discusses in some detail the area viewed by the BAO downward-facing pyranometer. Broken clouds, however, will introduce spatial sampling problems. Temporal sampling problems are also introduced because the tower data are available only as one-hour averages. Although the pixel measurements are temporally located in the same hour bins as the tower data, they nevertheless will refer to somewhat different solar zenith angles than represented by the hourly mean tower data. The transitory nature of clouds will introduce additional temporal sampling problems. It is anticipated that both spatial and temporal sampling problems are random. Additionally, the longer tower sampling time will partially compensate for the smaller viewing area when comparing to the satellite.

Summarized in Table 1 are the SW pixel measurements that have been collocated with the tower. As previously noted, emphasis is placed on measurements from ERBS, for which the clear pixels were identified according to the ERBE scene identification. A limited number of *NOAA-9* pixel measurements have also been collocated with the tower; their purpose will be elaborated in section 4 and does not require the identification of clear pixels. All measurements represent pixels that fall within a grid extending 0.3°N, 0.3°S, and 0.7°E of the tower. As discussed by Cess et al. (1991), this restriction to pixels located east of the tower is to avoid the foothills of the Rocky Mountains. If more than one pixel falls within this grid, the measurements are averaged.

TABLE 1. Summary of ERBE SW pixel measurements that have been collocated with the BAO tower.

Month	Clear	Total
	ERBS	
Apr 1986	2	26
May 1986	11	50
Jun 1986	1	15
Jul 1986	9	47
Aug 1986	1	16
Sep 1986	10	40
Jul 1987	20	45
Total	54	239
	NOAA 9	
Jun 1986	—	22
Jul 1986	—	23
Total	—	45

3. ECMWF GCM

For the purpose of comparing ECMWF GCM-generated fluxes with the collocated ERBE/tower measurements, simulations were performed with a spectral truncation of T106, corresponding to a $1\frac{1}{8}° \times 1\frac{1}{8}°$ Gaussian grid. The component of the model that is most germane to the present study is its SW radiation scheme, in particular that portion pertaining to clouds.

The SW radiation code in the ECMWF GCM is based on an updated version of the SW radiation model originally developed at the University of Lille (Fouquart and Bonnel 1980; Morcrette and Fouquart 1986; Morcrette 1991). It deals explicitly with a number of physical processes that often are neglected or empirically parameterized in other models, and it accounts for SW absorption by water vapor, oxygen, ozone, carbon dioxide, and cloud droplets. Multiple scattering by molecules (Rayleigh scattering) and clouds (Mie scattering) is treated in a rather explicit way. Interactions between scattering and molecular band absorption are dealt with by a photon path distribution method that separately takes into account the scattering and absorption processes; scattering is treated with the delta-Eddington approximation while transmission functions are developed as Padé approximants. Cloud SW radiative parameters are the optical thickness and single scattering albedo, both of which are functions of the cloud liquid water path, and a prescribed asymmetry factor (Fouquart 1987). These cloud SW radiation parameters have been fitted to in situ cloud measurements (Bonnel et al. 1983).

Convective precipitation is used as a cloud fraction predictor for convective clouds, with an upper limit of 80% cloudiness. For stratiform clouds the cloud fraction predictors are relative humidity, vertical velocity, and lapse rate.

4. Tower–ERBE Results

Attention is directed first to the dataset consisting of 239 ERBS pixel measurements, of which 54 are for clear skies, that have been collocated with the BAO tower. The 54 clear-sky tower/ERBS measurements, spanning a seven-month period (Table 1), exhibit similar behavior to the one-month (July 1987) dataset employed by Cess et al. (1991). The surface insolation, as measured by the upward-facing tower pyranometer, is linearly dependent on cos(solar zenith angle) as demonstrated in Fig. 1; this dependence is consistent with model calculations of the type discussed by Cess et al. (1991). Recall that these are hourly mean measurements, and they are for the hour bins within which the collocated ERBS data are contained. The modest scatter is primarily attributable to day-to-day variations in atmospheric water vapor content (Cess et al. 1991). The near-surface net downward SW radiation (tower) is, as in Cess et al. (1991), linearly correlated with that at the TOA (ERBS) as shown in Fig. 2 [a detailed discussion of this linear relationship is provided in Cess and Vulis (1989)]. The standard error is roughly twice that found in the earlier one-month study, because here no attempt was made to temporally correct the one-hour mean tower data to the ERBE data; that is, to correct for the time difference between the pixel measurements and the time that is representative of the one-hour tower averages. In that the focus of the present study is on the SW-radiative impact of clouds, and since the temporal correction procedure of Cess et al. (1991) is not applicable when clouds are present, we have treated the clear data in the same manner as we next treat the total data, so that no attempt was made to remove temporal sampling problems, which we anticipate to be random and thus compensatory.

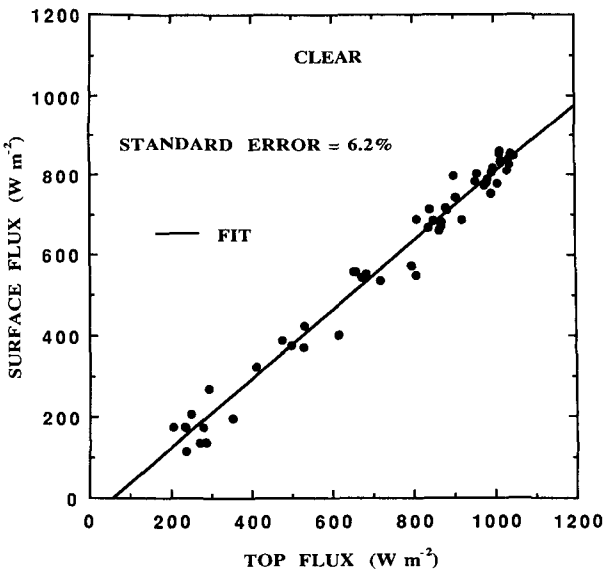

FIG. 2. Tower surface flux as a function of the ERBS TOA flux for the 54 clear-sky measurements.

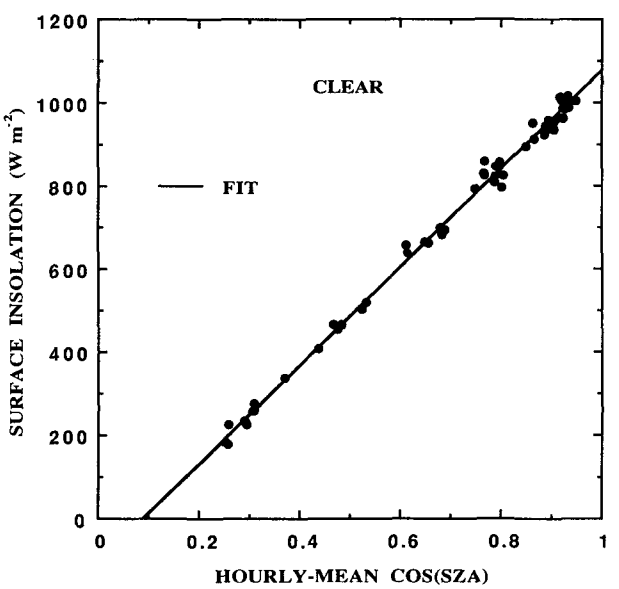

FIG. 1. Tower measurements of surface insolation as a function of the hourly mean cosine of the solar zenith angle (SZA). These represent the 54 clear-sky measurements.

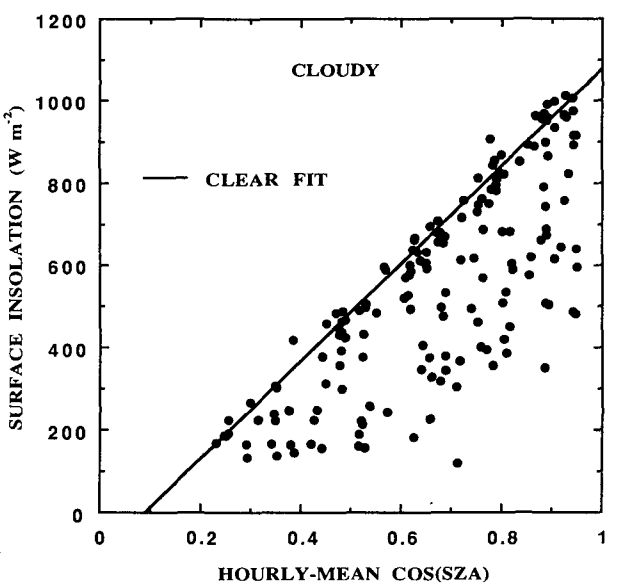

FIG. 3. Tower measurements of surface insolation as a function of the hourly mean cosine of the SZA. These represent the 185 cloudy (i.e., 239 total minus 54 clear) measurements.

Figure 3 is the same as Fig. 1 except for the 185 tower insolation measurements corresponding to those of the ERBS TOA, which bear the ERBE scene identifications of partly cloudy, mostly cloudy, or overcast: that is, 239 total ERBS measurements minus 54 clear measurements. As expected, in the mean clouds substantially reduce the surface insolation. What is somewhat surprising is the amount of data that lie on or near the clear fit taken from Fig. 1. There are four possible explanations. One is the occurrence of "invisible" cirrus, which could activate the ERBE longwave cloud identification algorithm but have essentially no impact on SW radiation. The second is that the area surrounding the tower is unusually bright (surface albedos range from 15% to 25% depending on solar zenith angle) for a vegetated surface, possibly causing the ERBE SW cloud identification algorithm to misidentify some clear pixels as cloudy pixels. Third, it is possible to have situations in which broken clouds are present in the ERBE pixel but not in the upward-facing pyranometer's smaller viewing area. And fourth, reflection from the sides of broken clouds might compensate for their reduction in direct radiation. Nevertheless, Fig. 3 demonstrates that clouds over the tower, on average, substantially reduce surface insolation.

Figure 4 is the same as Fig. 2 but includes all 239 collocated tower and ERBS measurements (clear plus cloudy). The threefold increase in standard error relative to Fig. 2 is consistent with enhanced temporal and spatial sampling problems caused by clouds as discussed in section 2. In the next section, however, it will be demonstrated that diurnal differences in cloud type can also introduce scatter into the data.

The intriguing point of Fig. 4 relative to Fig. 2 is

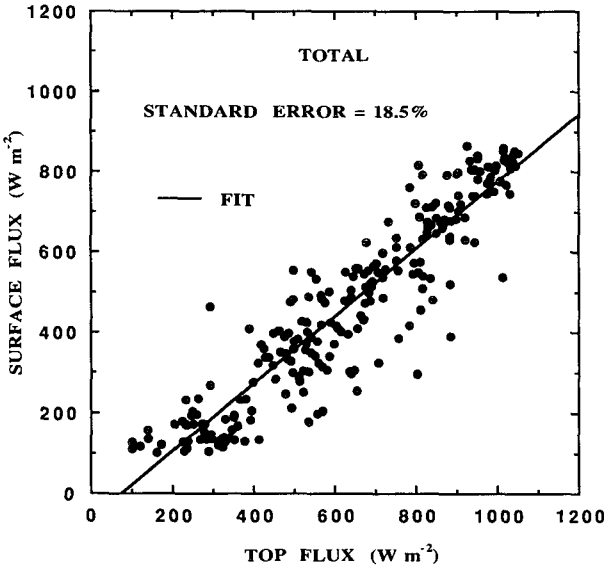

FIG. 4. Tower surface flux as a function of the ERBS TOA flux for the 239 total measurements.

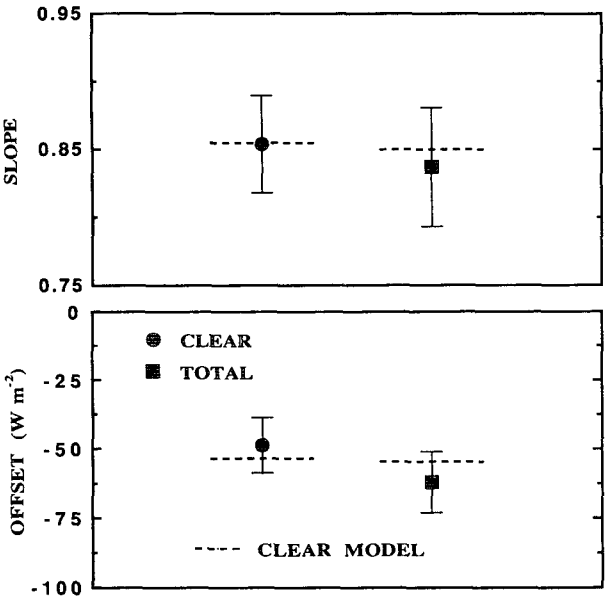

FIG. 5. Summary of slopes and offsets as determined from the 54 clear measurements, the 239 total measurements, and the clear-sky model. The precipitable water within the model is 1.22 cm for the clear simulation and 1.36 cm for the total simulation. The vertical bar denotes the 95% confidence interval.

that, in terms of the linear slope-offset relationship (Cess and Vulis 1989)

$$\mathrm{SURF} = A + B \times \mathrm{TOP}, \qquad (1)$$

where SURF and TOP denote the net downward SW radiation at the surface and at the TOA, clouds seem to have a minimal effect on the slope (B) and offset (A). This is clearly demonstrated by the comparisons shown in Fig. 5. But even if clouds were to produce no direct impact on the SURF versus TOP relationship, one might anticipate some difference caused by enhanced atmospheric water vapor on days when clouds are present relative to clear days. This effect is very slight, as demonstrated by using an atmospheric SW radiation model together with Stapleton Airport precipitable water measurements, both described by Cess et al. (1991). The surface albedo model for pasture land (Vulis and Cess 1989) was adopted within the model, since this is reasonably representative of the area surrounding the tower. Tropospheric aerosols and ozone were incorporated as in Cess et al. (1991). Averaged over days coinciding with the 54 clear measurements, the precipitable water above the tower is 1.22 cm, while for the total measurements it is 1.36 cm. This difference produces little effect on the model-produced slopes and offsets (Fig. 5).

It is important to fully understand the physical mechanisms that produce the slopes and offsets when collocating ERBS measurements with the tower, and to recall that ERBS provides sampling throughout the

diurnal cycle and, thus, over the diurnal range of solar zenith angles. For clear skies, variations in both SURF and TOP are produced primarily by variations in solar zenith angle (SZA), and denoting this slope by B_1, then

$$B_1 = \left| \frac{\partial(\text{SURF})/\partial(\text{SZA})}{\partial(\text{TOP})/\partial(\text{SZA})} \right|_{\text{clear}}. \quad (2)$$

As discussed by Cess and Vulis (1989), $B_1 < 1$ is the result of SW absorption by the atmospheric column. On the other hand, if SZA is held constant while cloudiness is allowed to vary, then it is cloudiness variations that produce changes in SURF and TOP; denoting this slope by B_2, then

$$B_2 = \left| \frac{\partial(\text{SURF})}{\partial(\text{TOP})} \right|_{\text{SZA}}. \quad (3)$$

The slope B_2 has a specific physical meaning. Absorption of SW radiation by the atmospheric column is TOP minus SURF, and it is easily shown that $B_2 > 1$ means that the addition of clouds to the atmospheric column produces SW radiative heating of the column and cooling if $B_2 < 1$. For example, if increased cloudiness produces a greater decrease in SURF than in TOP, then the absorption of SW radiation by the column (TOP minus SURF) is clearly increased, as is consistent with $B_2 > 1$ from (3).

With reference to the apparent agreement of slopes and offsets for the clear and total measurements (Fig. 5), it is important to recognize that the clear slope is the result of SZA variations (i.e., it is B_1), while the total slope is the combined result of SZA and cloudiness variations (i.e., it is a combination of B_1 and B_2). So it is possible that the total versus clear agreement in Fig. 5 may be coincidental. In fact, subdivision of the 239 total measurements into 120 morning and 119 afternoon measurements results in some degradation of this agreement (Fig. 6).

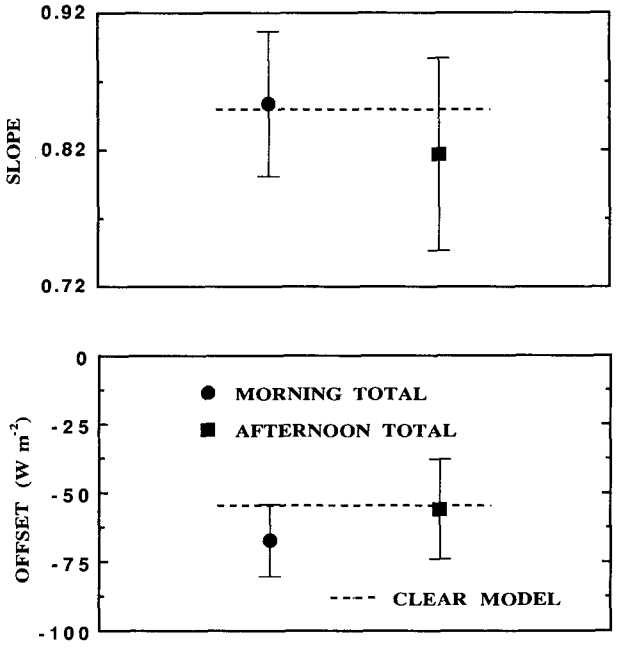

FIG. 6. Summary of slopes and offsets as determined from the 120 total morning measurements, the 119 total afternoon measurements, and the clear-sky model. The precipitable water within the model is 1.36 cm. The vertical bar denotes the 95% confidence interval.

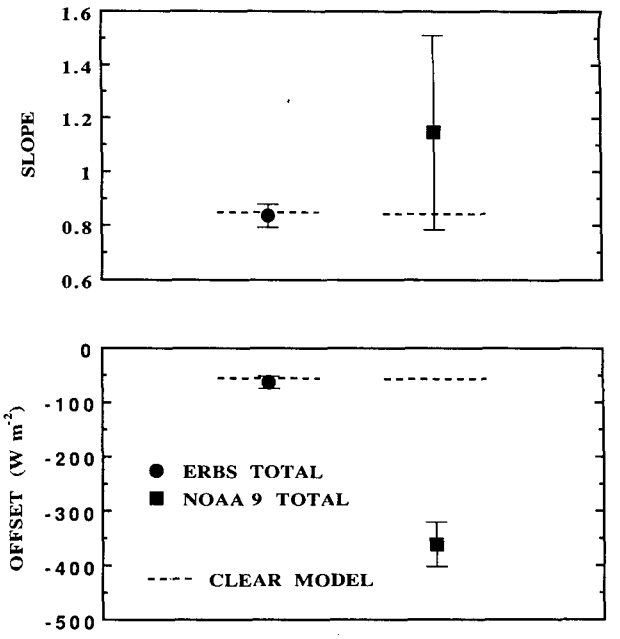

FIG. 7. Summary of slopes and offsets as determined using the 239 ERBS measurements, the 45 *NOAA-9* measurements, and the clear-sky model. The precipitable water within the model is 1.36 cm for the ERBS simulation and 1.61 cm for the *NOAA-9* simulation. The vertical bar denotes the 95% confidence level.

The 45 collocated *NOAA-9* measurements provide a very useful insight as to the possibility of coincidental slope agreement. Because *NOAA-9* is in a sun-synchronous orbit and the data are for June and July, variations in SZA are minimized so that the slope produced by the combined *NOAA-9* and tower measurements is a good approximation to B_2 as defined by (3). The slope and offset differ considerably from those inferred from the combined ERBS and tower data as demonstrated in Fig. 7. Recall that the *NOAA-9* mean measurement time is roughly 1400 LT.

Obviously, it would be useful if a dataset were available that provided sampling through all hour bins so that diurnal variability of the slope B_2 could be determined, in contrast to the *NOAA-9* single time of 1400 LT. Although ERBS does provide sampling in all hour bins, it does so in conjunction with seasonal variability of SZA and thus does not provide an estimate of B_2. To better understand the combined ERBE and tower data, as well as to demonstrate the usefulness of a more

comprehensive dataset, we next use the ECMWF GCM to generate a surrogate dataset.

5. ECMWF GCM results

Before the ECMWF GCM is employed as an aid to understanding the tower/ERBE data, these measurements will be used to demonstrate one means of validating the GCMs SW radiation code with particular emphasis on the model's cloud radiation properties. Two perpetual-month simulations, April and July, were performed with output taken from a single grid located at 39.81°N, 104.63°W as representative of the tower location. Radiation was sampled every three hours within the GCM, and the two perpetual-month simulations produced 217 total time samples, of which 55 are for clear skies. These numbers are quite similar to the combined tower/ERBS data (239 and 54 respectively). Both the GCM output and the tower/ERBS data were screened to exclude surface fluxes less than 100 W m^{-2} to be consistent with (1) (see Fig. 12 of Cess and Vulis 1989).

Figure 8 compares the 55 clear-sky SURF and TOP outputs from the GCM to the tower/ERBS linear fit from Fig. 2; the mean error of the model relative to the data is only 3%. Agreement between the GCM and either of the two separate datasets (i.e., ERBE or the tower) would not be as good, because the model's surface albedo (about 11%) is considerably less than that of the vicinity of the tower. The important point is that the SURF versus TOP relationship is quite insensitive to surface albedo (Cess and Vulis 1989), so that the comparison in Fig. 8 serves as a direct test, for clear skies, of the atmospheric component of the model's SW radiation code.

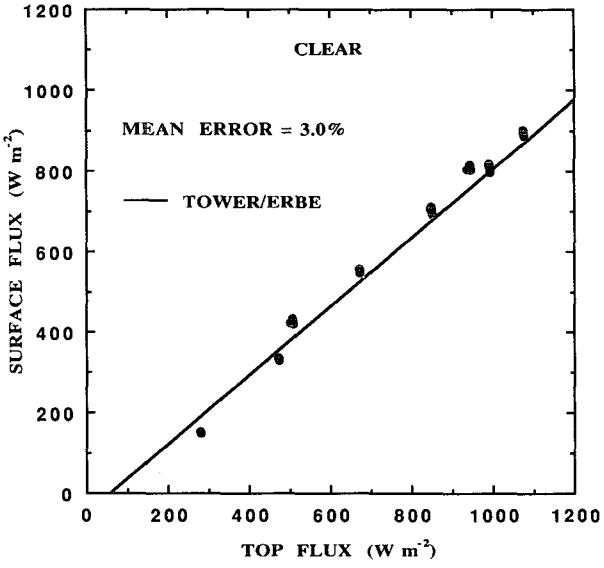

FIG. 8. The ECMWF GCM surface flux as a function of the TOA flux for the combined perpetual April and July simulations. These are for the 55 clear-sky outputs. The mean error is referenced to the corresponding tower/ERBS regression from Fig. 2.

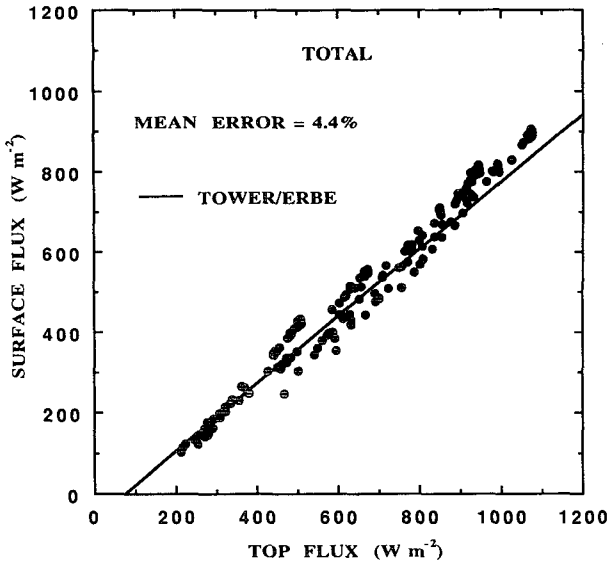

FIG. 9. The ECMWF GCM surface flux as a function of the TOA flux for the combined perpetual April and July simulations. These are for the 217 total outputs. The mean error is referenced to the corresponding tower/ERBS regression from Fig. 4.

This is likewise true of the comparison of total output to the data fit of Fig. 4, as shown in Fig. 9. Like the tower/ERBS data, there is little difference in the GCM slopes and offsets of Figs. 8 and 9, indicating that cloud amount has a minimal impact on the GCM's relationship between SURF and TOP. This is important, because if a model were compared against either of the two individual datasets, one could not distinguish between errors caused either by cloud radiative properties or by cloud amount. The comparison to the coupled dataset thus serves to isolate cloud radiative properties, and as will be demonstrated, this implicitly includes cloud type. The agreement in Fig. 9 is comparable to that for clear skies (Fig. 8), and this serves as one means of validating the GCM's SW cloud radiative properties. This is consistent with a related study by Slingo et al. (1992). They demonstrated that perpetual January and July simulations with the ECMWF GCM produce realistic diurnal variations in the TOA outgoing longwave radiation, indicating that the model has a realistic diurnal cycle of cloudiness.

An interesting aspect of Fig. 9 is that there is considerable scatter, suggesting that the data scatter in Fig. 4 might be caused by more than spatial and temporal sampling problems. The GCM scatter (Fig. 9) is, in fact, caused by diurnal variability of the cloud-induced slope B_2, as the *NOAA-9* data suggest. To demonstrate this, we concentrate on the perpetual July results shown in Fig. 10. Illustrated in Figs. 11 and 12 are output for the individual sampling times together with their respective slopes B_2. The point is that these B_2 slopes

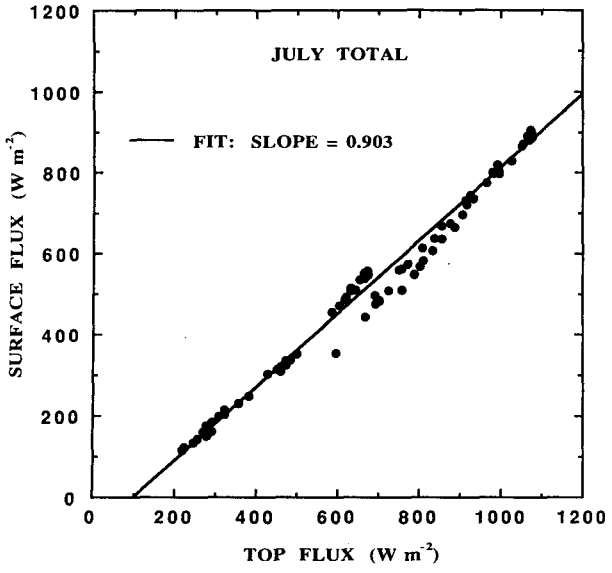

FIG. 10. The ECMWF GCM surface flux as a function of the TOA flux for the total outputs from the perpetual July simulation.

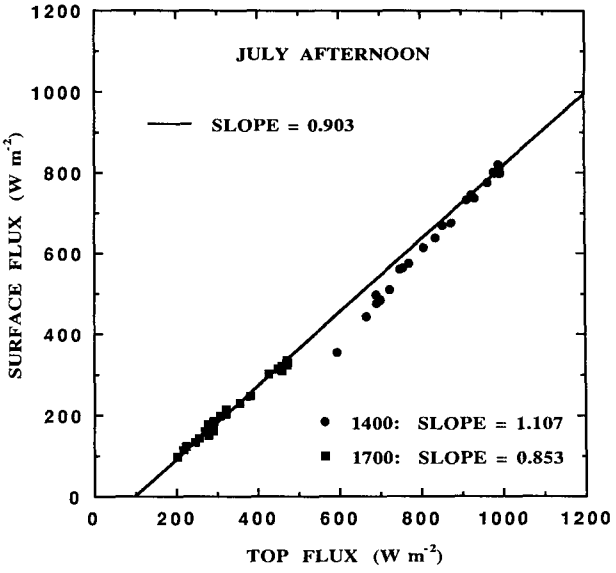

FIG. 12. As in Fig. 10 but with restriction to afternoon sampling times (1400 and 1700 LT).

have diurnal variability and differ from the slope generated by the total output (0.903 from Fig. 10). Thus, it is the time-dependent B_2 slopes that are the cause of scatter in Fig. 10, and presumably, this is the cause of some of the scatter in the dataset (Fig. 4). It is emphasized that this diurnal variability of B_2 refers to a specific geographical region.

As noted by Slingo et al. (1992), the ECMWF GCM produces realistic diurnal variations in the TOA outgoing longwave radiation, indicating that the model has a realistic diurnal cycle of cloudiness.

The GCM B_2 values are also intuitively consistent with diurnal changes of cloud type in the Boulder area for July. Typically morning clouds are low stratus that enhance upward-reflected SW radiation through the atmosphere and so radiatively heat the atmospheric column, resulting in $B_2 > 1$ as is consistent with Fig. 11. The predominate cloud type in the late afternoon is residual cirrus caused by afternoon convective activity. Cirrus clouds deplete SW radiation reaching the underlying atmosphere, thus cooling the atmospheric column so that $B_2 < 1$ as is consistent with the 1700 LT slope in Fig. 12. Note also that the GCM-generated $B_2 = 1.107$ at 1400 LT (Fig. 12) is comparable to that determined from *NOAA 9* at essentially the same time (Fig. 7), although there is considerable uncertainty in the *NOAA-9* slope.

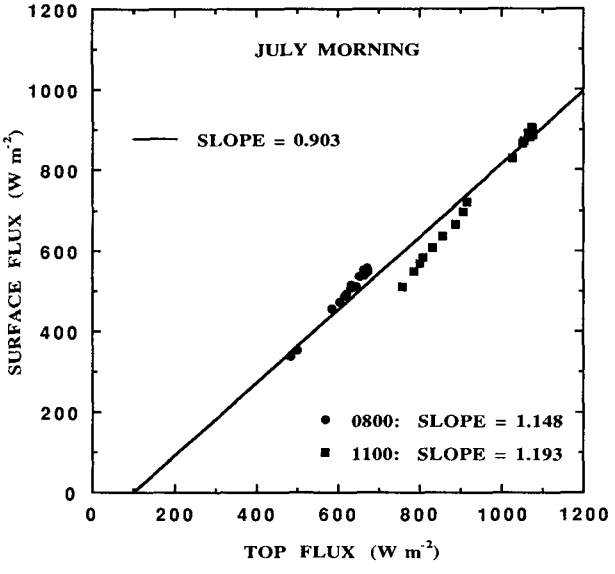

FIG. 11. As in Fig. 10 but with restriction to morning sampling times (0800 and 1100 LT).

6. Surface retrieval

In addition to the question of the SW radiative impact of clouds on the atmospheric column, the tower/ERBS dataset serves a second purpose: the applicability of (1) as a retrieval algorithm for determining SURF when given TOP from satellite measurements. The use of (1) as a clear-sky algorithm has been discussed by Cess and Vulis (1989) and Cess et al. (1991). The question here concerns the possible applicability of the clear-sky algorithm to cloudy-sky conditions. To address this issue, the 239 ERBS TOP measurements have been employed to determine SURF from the clear-sky algorithm, and these are then compared to the tower measurements. For this purpose the clear-sky values

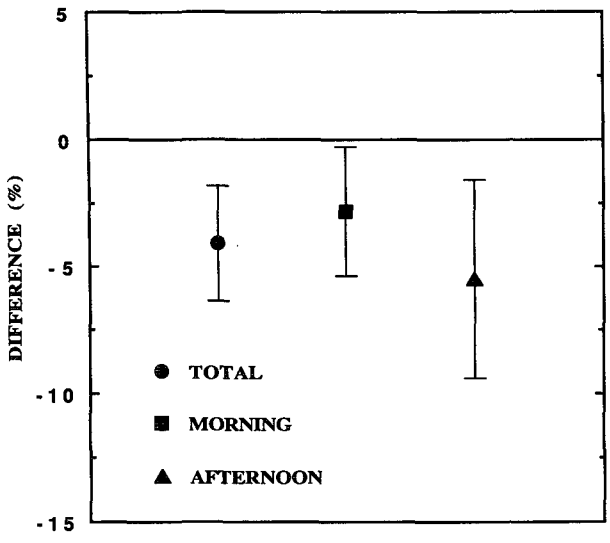

FIG. 13. Differences between the 239 tower measurements of SURF and SURF as evaluated from the 239 collocated ERBS measurements employing the clear-sky retrieval algorithm. The vertical bar denotes the 95% confidence interval.

of A and B have been determined from the 54 collocated tower/ERBS clear-sky measurements and then corrected, using the atmospheric SW radiation model, for the modest difference in precipitable water between clear and total days. In the context of Fig. 5, A and B are the clear tower/ERBS values, but with a small negative correction determined from the clear-sky model to account for the difference between 1.36 cm (total days) versus 1.22 cm (clear days) of precipitable water. This correction amounts to only −0.8%.

Differences of SURF determined from the actual tower measurements relative to the clear-sky algorithm are shown in Fig. 13. Note that clouds produce a modest negative bias for the 239 total measurements, and that this persists when the dataset is divided into morning and afternoon measurements, although the morning bias is somewhat diminished. While these negative biases are small, they are significant enough to suggest that some explicit accounting for clouds will be required when attempting to infer, from satellite measurements, the net downward SW flux at the surface.

7. Concluding remarks

The present study has addressed two separate but related issues: What is the SW radiative impact of clouds on the atmospheric column, and how do clouds influence a linear slope-offset retrieval algorithm for determining, from satellite measurements, the net downward SW radiation at the surface? The collocated tower/ERBE data were only marginally useful in addressing the first issue; the June and July collocated *NOAA-9* measurements demonstrated for these months that the SW radiative impact of clouds in the vicinity of Boulder leads to heating of the atmospheric column in the early afternoon. It was, however, shown that output from the ECMWF GCM agreed well with the tower/ERBE datasets, a consistency that serves as one means of validating the GCM's cloud radiation properties. Of equal importance is that the GCM interpretation demonstrated what could be done with a more comprehensive dataset.

For example, the high temporal sampling rate of the GOES spin-scan radiometer could provide such a dataset, particularly if a June–July period was chosen so as to minimize variations in solar declination angle and thus solar zenith angle. In principle, this would yield data similar to the present tower/*NOAA-9* collocation, but for all hour bins throughout the day so as to provide diurnal variability of the slope B_2 and thus of the SW radiative impact of clouds on the atmospheric column. Such a dataset would serve as an even more stringent test of SW radiation in a GCM than do the present datasets. Although the GOES SW radiometer is a narrowband and uncalibrated instrument, combined narrowband to broadband conversion and calibration could be achieved through calibration of GOES measurements to collocated ERBE pixel measurements in the vicinity of the tower.

With respect to the second issue, it has been shown, relative to a linear clear-sky retrieval algorithm, that clouds produce small but marginally significant negative biases in the net downward SW radiation at the surface. This suggests that some explicit accounting for clouds will be required when attempting to infer, from satellite measurements, the net downward SW radiation at the surface. Moreover, these biases as shown in Fig. 13 should not be regarded as indicative of regions other than the tower vicinity. One might anticipate quite different conclusions over ocean areas because of the much lower surface albedo relative to the tower area.

Acknowledgments. The Boulder aerosol optical depth data were supplied by Pat Reddy. Don Nelson assisted in the operation and calibration of the tower instruments, and Lisa Corsetti assisted in the GCM simulations. This work was supported by DOE Grants DEFG0285ER60314 and DEFG290ER61603, NASA Grants NAS118155 and NAG11264, and NSF Grant ATM8815885, all to SUNY Stony Brook, and by DOE Contract W-7405-Eng-48 to the University of California.

REFERENCES

Bonnel, B., Y. Fouquart, J.-C. Vanhoutte, C. Fravalo, and R. Rosset, 1983: Radiative properties of some African and mid-latitude stratocumulus clouds. *Contrib. Atmos. Phys.*, **56**, 409–428.

Cess, R. D., and I. L. Vulis, 1989: Inferring surface solar absorption from broadband satellite measurements. *J. Climate*, **2**, 974–985.

——, E. G. Dutton, J. J. DeLuisi, and F. Jiang, 1991: Determining

surface solar absorption from broadband satellite measurements for clear skies: Comparison with surface measurements. *J. Climate,* **4,** 237–247.

——, and Co-authors, 1990: Inter-comparison and interpretation of climate feedback processes in 19 atmospheric general circulation models. *J. Geophys. Res.,* **95,** 16 601–16 615.

Dutton, E. G., 1990: Annual forcing of the surface radiation balance diurnal cycle measured from a high tower near Boulder, Colorado. *J. Climate,* **3,** 1400–1408.

Fouquart, Y., 1987: Radiative transfer in climate modeling. NATO Advanced Study Institute on Physically Based Modeling and Simulation of Climate and Climate Changes, Erice, Sicily. M. E. Schlesinger, Ed., 223–283.

——, and B. Bonnel, 1980: Computations of solar heating of the earth's atmosphere: A new parameterization. *Contrib. Atmos. Phys.,* **53,** 35–62.

Harrison, E. F., P. Minnis, B. R. Barkstrom, V. Ramanathan, R. D. Cess, and G. G. Gibson, 1990: Seasonal variation of cloud radiative forcing derived from the Earth Radiation Budget Experiment. *J. Geophys. Res.,* **95,** 18 687–18 703.

Morcrette, J.-J., 1991: Radiation and cloud radiative properties in the European Centre for Medium Range Weather Forecasts Forecasting System. *J. Geophys. Res.,* **96,** 9121–9132.

——, and Y. Fouquart, 1986: The overlapping of cloud layers in shortwave radiation parameterizations. *J. Atmos. Sci.,* **43,** 321–328.

Ramanathan, V., R. D. Cess, E. F. Harrison, P. Minnis, B. R. Barkstrom, E. Ahmad, and D. Hartmann, 1989: Cloud–radiative forcing and climate: Results from the Earth Radiation Budget Experiment. *Science,* **243,** 57–63.

Slingo, J. M., K. R. Sperber, J.-J. Morcrette, and G. L. Potter, 1992: Analysis of the temporal behavior of convection in the tropics of the ECMWF model. *J. Geophys. Res.,* submitted.

Vulis, I. L., and R. D. Cess, 1989: Interpretation of surface and planetary directional albedos for vegetated regions. *J. Climate,* **2,** 986–996.